Additive Manufacturing 70 (2023) 103546

Contents lists available at ScienceDirect

Additive Manufacturing

journal homepage: www.elsevier.com/locate/addma

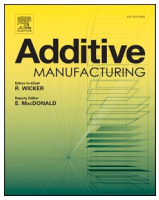

Research paper

5-axis multi-material 3D printing of curved electrical traces

Freddie Hong [a,*], Borut Lampret [a], Connor Myant [a], Steve Hodges [b], David Boyle [a]

[a] Imperial College London, London, United Kingdom
[b] Microsoft Research, Cambridge, United Kingdom

ARTICLE INFO

Keywords:
5-axis 3D printing
3D printed electronics
Conductive filament
Rapid prototyping

ABSTRACT

Prototyping three-dimensional (3D) printed electronics via material extrusion (MEX) has become popular in recent years with the increased availability of commercial conductive filaments. However, the current planar 3D printing method of layer upon layer construction shows clear challenges in extruding conductive traces for inclining surfaces. This inherent limitation of planar 3D printing restricts the design freedom of 3D printed electrically conductive objects with conductive filaments based on Polylactic Acid (PLA). To overcome this limitation of planar 3D printing, this paper describes a novel method of employing a multi-material 5-axis 3D printer to extrude conductive PLA in curved layers. The paper characterises changes in the resistivity of printed traces for angles of incline and curvatures using two commercial conductive PLA filaments. Conductive traces were printed via a custom-built desktop 5-axis 3D printer and a conventional multi-material MEX 3D printer. We found that 3D printing following a conformal approach can reduce the resistivity of the vertical conductive trace by more than 9 times. The paper concludes by successfully fabricating complex conductive patterns onto free-form doubly curved substrates.

1. Introduction

Integrating conductive elements in three-dimensional (3D) printing is gaining popularity with the increased availability of 'extrudable' conductive materials. 3D printing electronics offers a new range of opportunities for rapid prototyping of interactive devices, such as increased freedom of design, miniaturisation of circuit boards, reduced time and cost of constructing bespoke prototypes. Various approaches to integrating electrical features into 3D printed parts have been reported in the literature, such as the ultrasonic embedding of wires into 3D printed parts [1,2], material extrusion and material jetting of conductive silver ink [3–6], and material extrusion of conductive Polylactic Acid (PLA) filaments [7]. However, all the above methods for 3D printing conductive traces have a common limitation of fabricating conductive elements for inclining surfaces, which largely restricts the design freedom beyond the XY plane [8]. This is due to the inherent character of the planar construction, where the materials are deposited layer upon layer causing weaker conductivity or broken inter-layer bonding of interconnects on inclining surfaces [8].

As a method of circumventing this problem, various approaches to 3D printing conformal circuits have been explored, such as transferring prefabricated planar circuit patterns via additive stamping [9], hydroprinting [10–12], thermoforming [13,14], non-planar extrusion of carbon nanotube-based composite [40,41] or material extrusion of conductive ink on a multi-axis stage [15,16]. However, no approach of using conductive PLA on a multi-axis material extrusion (MEX) 3D printer has been reported to-date. Among various other methods, MEX is the most popular form of 3D printing for different user groups because the machine and the material are low cost and easy to use. In this work, two commercially available examples of conductive PLA materials were 3D printed onto various inclined and curved 3D printed substrates using a custom multi-material 5-axis MEX 3D printer. After experimenting with the resistance of single-line conductive traces, we 3D printed more complex conductive patterns onto a doubly curved substrate with arbitrary form factors to demonstrate the design and fabrication capabilities of a desktop multi-material 5-axis 3D printer to produce curved circuits. Conformal 3D printing has been successfully demonstrated in the literature using multi-axis computer-numerically controlled (CNC) machines and 6 degrees of freedom robotics arms with a filament extrusion head [17–19]. These machines, however, are out of reach for most individual users due to the high cost and the technical knowledge required for operating the machine. In addition, since these machines are not designed for 3D printing specifically, they are not compatible with most other popular 3D printing firmware and controllers. In recent years,

* Corresponding author.
E-mail address: t.hong19@imperial.ac.uk (F. Hong).

https://doi.org/10.1016/j.addma.2023.103546
Received 5 December 2022; Received in revised form 20 March 2023; Accepted 7 April 2023
Available online 11 April 2023
2214-8604/© 2023 The Authors. Published by Elsevier B.V. This is an open access article under the CC BY-NC license (http://creativecommons.org/licenses/by-nc/4.0/).

various affordable and 'desktop friendly' 5-axis 3D printers have been introduced to allow individual designers, makers and hobbyists to be on board with multi-axis 3D printing [20–23]. One of the biggest barriers to employing multi-axis 3D printing is the difficulty of accessing or developing a slicer that can generate a curved toolpath. Some researchers have adapted multi-axis slicing algorithms through numeric computing environment [24,25,42,43], while others have used 3D modelling software with visual scripting extensions, e.g., Rhinoceros and Grasshopper [26], to design and produce the G-code [20,27,28]. Visual scripting environments offer designers the ease of rapidly prototyping complex geometries and the capability to evaluate the design and create parametric systems without much scripting knowledge. This paper combines state-of-the-art 5-axis 3D printing and 3D printing of electronics to invite more researchers and makers into 3D printing curved electronics.

2. Material and methods

2.1. Conductive PLA

Two specific examples of commercially available conductive 1.75 mm PLA filaments have been used in this work: a carbon-based PLA called ProtoPasta and a copper-based PLA called Electrifi [30]. The two filaments were selected because they show distinctive advantages and disadvantages over one another. Firstly, ProtoPasta has much higher resistivity. ProtoPlant advertises ProtoPasta's resistivity as 300 Ω·mm in the XY plane and 1150 Ω·mm along the Z axis [29] (although values reported in literature show 60 Ω·mm in the XY plane and beyond 200 Ω·mm along the Z axis [38,39]) compared to Electrifi's resistivity of 0.12 Ω·mm in the XY plane and 0.85 Ω·mm along the Z axis [7]. ProtoPasta can, however, be printed at a much higher temperature (210 °C), which means it can be extruded more easily without requiring fine adjustments to print settings. In contrast, Electrifi is highly susceptible to 3D printer settings and thermal environmental conditions [31]. Electrifi should be printed at a low temperature (145 °C), as otherwise its conductivity drops significantly. The lower printing temperature also contributes to weaker bonding between layers. In this work, substrates were 3D printed at 220 °C using a standard non-conductive PLA filament (1.75 mm).

2.2. 5-axis 3D printer

To fabricate the conformal samples, we built a custom multi-material 5-axis 3D printer based on E3D's tool-changer hardware [32] (Fig. 1). Employing tool-changing methods over a conventional dual-nozzle extrusion head was vital because any additional volume on the extruding head increases the contact angle, which limits the freedom of the design. There are two approaches to multi-axis 3D printing: i) rotating the print bed or ii) rotating the extruding head. In our version of the 5-axis machine, we employed the rotary bed approach because: i) Since the nozzle is fixed vertically, the material is always extruded downward, working in concert with gravity; ii) The rotary bed does not need to unwind the wire and therefore the rotary bed approach can use shortest tool-paths for faster printing; and iii) Since the rotary bed is independent of other axes, it can fit into various other Cartesian machines for an easy conversion of a 3-axis machine into a 5-axis machine. A simple method of converting a Cartesian 3D printer into a 5-axis 3D printer has been shown by Hong et al. [20]. The two-axis rotary bed shown in this paper was built with 3D printed components. Rotary beds used for 3D printing do not require the same degree of rigidity as the ones in multi-axis milling, therefore we found that 3D printed hardware was structurally adequate. The rotary bed was fitted onto the Z-axis gantry of the core XY-type 3D printing mechanism. Our multi-material 5-axis 3D printer is controlled with the popular Duet3D Duet 2 WiFi and Ethernet 3D printing control board [33] and RepRap firmware [34]. We openly share the hardware design and controller firmware of our custom 5-axis 3D printer in a GitHub repository.[1] We also employed an elongated 0.4 mm nozzle from nonplanar.xyz to reduce the contact angle between the extruding head and the PLA substrate, and thus provides a greater degree of freedom in curved extrusion.

2.3. 5-axis slicing

To construct the conformal traces, we employed an openly available slicer, Open5x [20], that is based on Rhinoceros/Grasshopper. Since Open5x is implemented into the CAD environment, it also provides visualisation of the printing process which is helpful in detecting potential collisions. Fig. 2A) shows a simulated movement of the 5-axis 3D print for the vase-like structure and 2B) shows the actual printing process. In the slicer, the retraction height can also be checked and adjusted to prevent collisions. The 5-axis 3D printing process of the vase-like samples presented in this paper can be found in the video Fig. 1.

Supplementary material related to this article can be found online at doi:10.1016/j.addma.2023.103546.

3. Experiments

To investigate the effect of curved layer deposition in 3D printing of electrical traces, we compared the differences in resistivity of the conformally and planarly 3D printed electrical traces for various angle of incline and curvature radii (Fig. 3). Both the planar and conformal samples were printed on same 3D printer with the elongated nozzle. The conformal samples were printed on the 5-axis stage and the planar samples were printed on the 3-axis stage. After the initial investigation, we fabricated more complex conductive patterns on a doubly curved substrate with arbitrary form factors. We predicted the resistance of each pattern in the results section using the resistivity measured from the inclined and curved samples.

We calculated the resistivity of the 3D printed traces with the following equation: $\rho = RA/l$, where R is the electrical resistance of the trace, A is the cross-sectional area of the trace and l is the length of the trace. Resistances of the printed traces were measured using a multimeter (77IV, Fluke). We applied a conductive silver ink (L100, Kemo) onto the contact pads of the traces to minimise the contact resistance. The conductive ink used in this paper has sheet resistance of 0.02–0.1 Ω/cm^2. The ink was left to cure at room temperature for 24 h. The designed dimensions of the conductive trace were used to determine resistivity, and measurements of the cross-sectional area of the printed traces were taken to verify its accuracy. Measurements were taken by cutting the samples perpendicularly to the direction of the trace and taking an image of the profile with a BDS400 optical microscope (Fig. 10).

3.1. Inclined substrate

To test the changes in resistivity of 5-axis 3D printed traces, we 3D printed three conductive traces onto seven right-angled triangle substrates with inclines varying from 15 to 105 degrees in 15-degree increments, which were 3D printed in the planar approach. The 105-degree incline is an undercutting surface, which is impossible to print with non-planar conformal printing via a 3-axis stage [24,35]. The 5-axis 3D printing process begins by first 3D printing a white PLA substrate in planar onto the rotary bed. We printed the substrate triangle and the conductive trace with a 0.3 mm layer height using a 0.4 mm nozzle and without bed heating. Once complete, the 5-axis machine swaps the extrusion head for conductive PLA. Then, on top of the substrate, three traces of conductive PLA traces were printed with 0.6 mm width, 1.2 mm depth and 40 mm length, with additional contact pads at each end of the trace. The extruding temperature was 145 °C for Electrifi

[1] http://www.github.com/FreddieHong19/Open5x

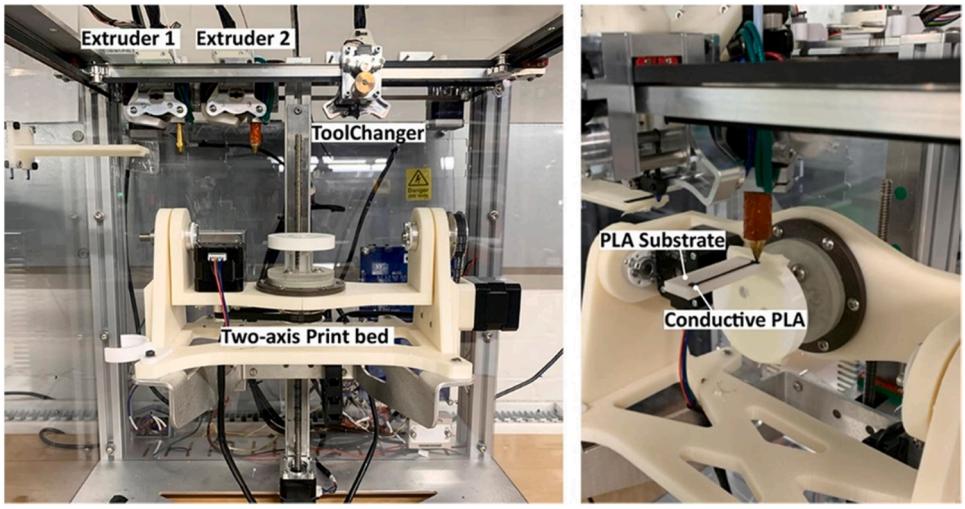

Fig. 1. Left: Customised multi-material 5-axis 3D printer based on E3D's Tool-changer hardware system. Right: 5-axis 3D printing of process of a conductive trace onto an inclined substrate.

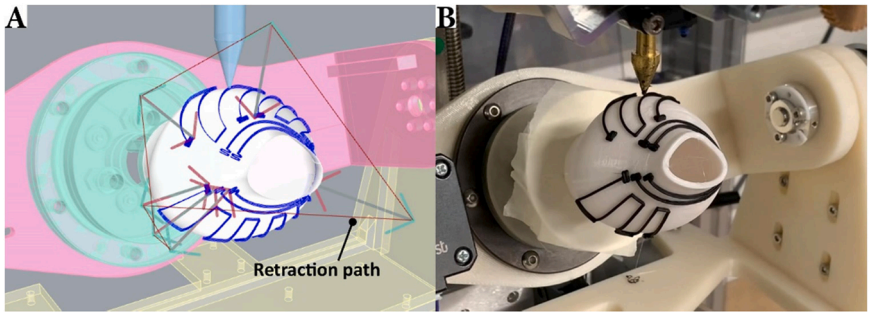

Fig. 2. 5-axis 3D printing vase-like object with conformal traces. A) Visualisation of the 5-axis printing process on Open5x slicing environment. Blue line indicates the printing path, the green and red lines indicate the travel path for retraction and de-retraction. B) Actual printing process of the conductive trace on the vase-like object.

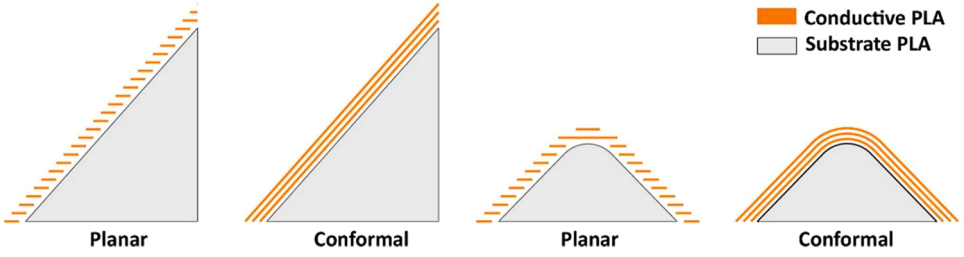

Fig. 3. Illustration of the planar and conformal printing path for inclined substrate (left) and curved substrate (right).

and 210 °C for ProtoPasta. The print settings were identical for both the planar and conformal samples.

3.2. Curvature radius

For 3D printing of the curved samples, we used identical print settings as for the inclines for both substrates and traces. We 3D printed the curved substrates with each including a segment with a constant radius of curvature ranging from 0 to 10 mm with 2 mm increments.

3.3. Conductive pattern on doubly curved surface

We tested 5-axis 3D printing on more complex conductive patterns on a free-form, doubly curved vase-like substrate to demonstrate the capability of 5-axis 3D printing for constructing conformal circuits. The bounding size of the substrate is 50 mm by 45 mm in the plane, and 60 mm in height. We printed six traces with different patterns and lengths on the substrate. Each trace has a different travel pattern and a different relationship with the substrate's layers. The resistance of each conductive trace was predicted by using values retrieved from the inclined and curved samples. Fig. 4 shows the six different conductive patterns on the doubly curved vase-like substrate. Each pattern has the same trace profile as the earlier tests. The length of each pattern is 116 mm, 93 mm, 115 mm, 131 mm, 79 mm and 69 mm, respectively.

4. Result and discussion

As mentioned in the Introduction, many of the failures in 3D printing

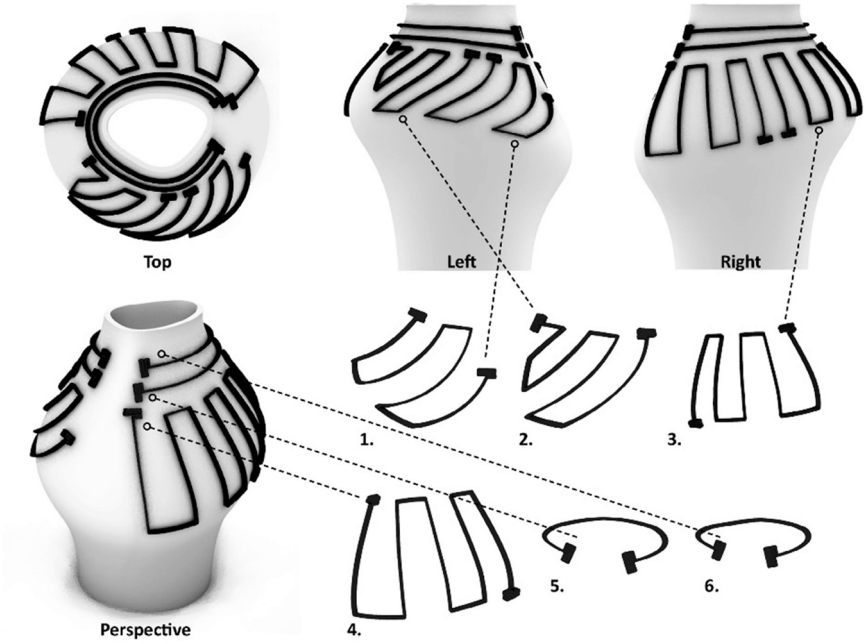

Fig. 4. Rendered diagram of the six conductive patterns on doubly curved vase-like substrate.

occur in between the layers where the inter-layer bonding is dependent on the surface adherence of the PLA. The weak adherence can lead to print delamination and failure, especially for delicate features such as electrical traces. Multi-material 3D printing can also cause cross-contamination of the materials caused by stringing and oozing. For 3D printing of conductive traces, this can also lead to a short circuit between the traces.

4.1. *Effect of 5-axis 3D printing on inclining surfaces*

Fig. 5 shows the carbon-based PLA 3D printed via A) conformal and B) planar approaches. Visually, the conformal samples have a higher finish quality with no evidence of oozing or stringing. The resistivity of the carbon-based PLA printed in planar (black) and conformal (red) is shown in Fig. 6. As shown in the graph, the resistivity of the planarly 3D printed samples increases with the angle of incline. Higher degree of incline means more print layers, which in turn means that the resistivity of the planarly printed traces relies more on inter-layer bonding than intra-layer bonding, which results in poorer conductivity of the traces [36]. The relationship between the angle of incline and resistivity is evident in the graph, in which it is shown that the 105-degree sample has a lower resistivity than the 90-degree sample despite overhanging. The number of printed layers for each angle of incline is shown in Table 1. Compared to the planar traces, the conformal traces show a significantly smaller trend of resistivity increasing with the angle, most likely a result of the planar traces consisting of more intra-layer than interlayer connections. Fig. 7 shows a comparative microscopic image between the planar and conformal samples for the 45-degree incline. Comparative microscopic images for the other angles can be found in Fig. S1 in the SM. The planar sample relies much more on inter-layer bonding, whereas the conformal sample relies more on intra-layer bonding. The resistivity of the 0-degree trace was 84 Ω·*mm*. The difference between the highest and lowest resistivity of the carbon-based planar sample was 197 Ω·*mm*, and 16 Ω·*mm* for the conformal sample.

Fig. 8 shows the copper-based PLA 3D printed via A) conformal and B) planar approaches. The copper-based PLA employed in our experiment is generally more challenging to 3D print than carbon-based PLA. This is mostly due to the rheological properties of the copper-based PLA

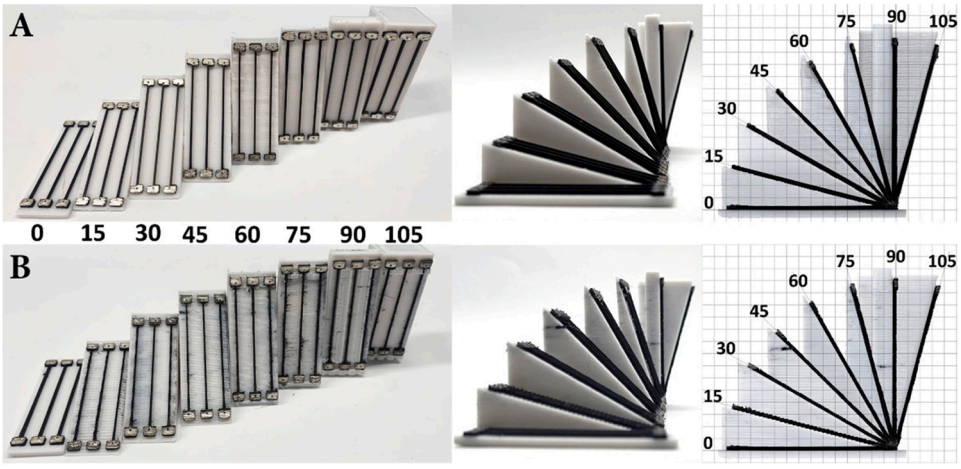

Fig. 5. Carbon-based conductive traces printed onto an inclined substrate with the angle ranging from 0 to 105 degrees. (Left) Front view, (Middle) side view, (Right) orthogonal view with grid: A) samples printed via conformal approach and B) samples printed via planar approach.

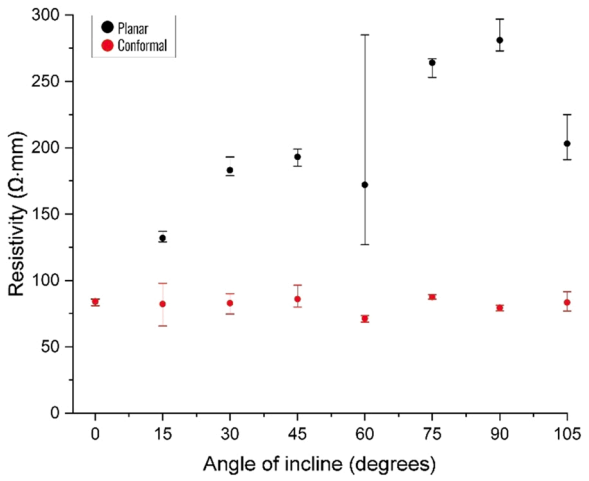

Fig. 6. The average resistivity of the printed carbon-based PLA traces versus the angle of incline. Planarly printed samples are in black and conformally printed samples are in red. The error bars indicate the range of measured values for the respective angle of incline.

Table 1
Incline angle and the number of substrate layers under conductive traces.

Angle (deg)	0	15	30	45	60	75	90	105
Number of layers	4	44	80	110	134	148	152	148

and weaker adhesive bonding than carbon-based PLA. As shown in Fig. 9, the resistivity of the planarly 3D printed copper-based trace also increases with the angle of incline. This trend is very similar the trend observed with the carbon-based PLA, where the increase in the reliance on inter-layer bonding also increases the resistivity. However, differently to the carbon-based sample, the copper-based sample shows a much greater relative increase in resistivity between inclines. We

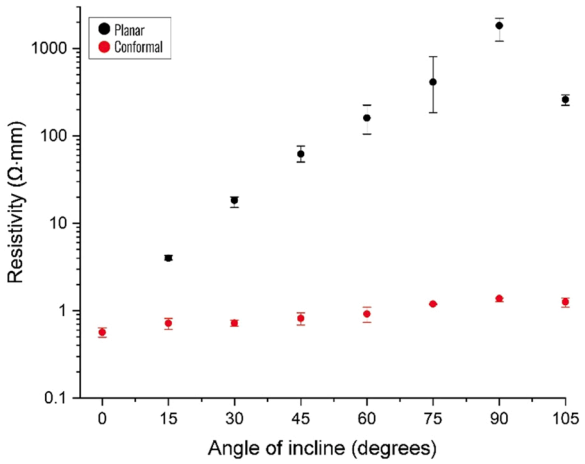

Fig. 9. The average resistivity of the printed copper-based PLA traces versus the angle of incline. Planarly printed samples are in black and conformally printed samples are in red. The error bars indicate the range of measured values for the respective angle of incline.

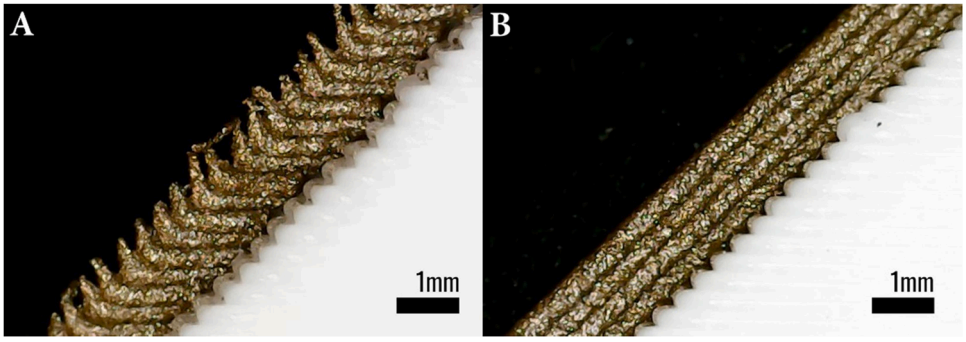

Fig. 7. Microscopic images of conductive traces printed on a 45-degree incline via A) planar approach, and B) conformal approach.

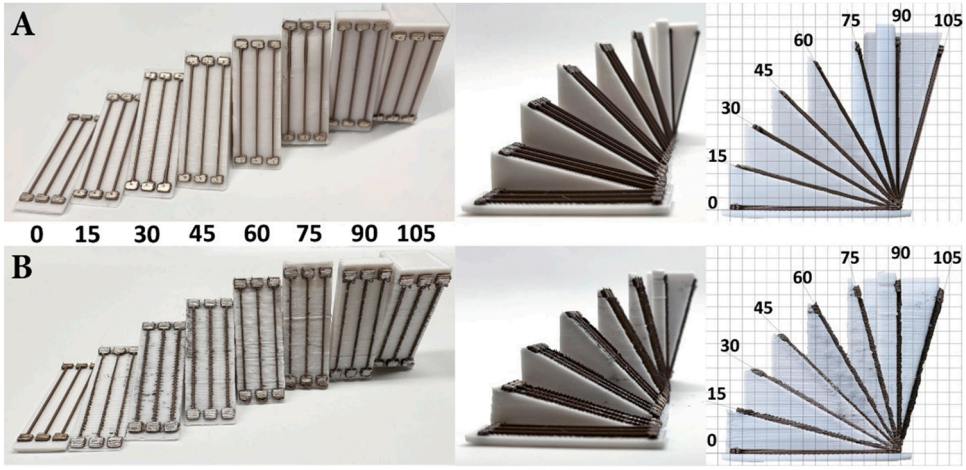

Fig. 8. Copper-based conductive traces printed onto an inclined substrate with an angle ranging from 0 to 105 degrees. (Left) Front view; (Middle) side view; and (Right) orthogonal view with grid. A) samples printed via conformal approach, and B) samples printed via planar approach.

suspect this is due to an additional factor that is independent to the geometry factor, reducing the conductivity of the printed trace. We suspect that a major contributor is the thermal annealing of the copper-based traces caused by both the travel of the heated substrate PLA nozzle ($220^{\circ}C$) near the printed traces and its nearby deposition of hot PLA. Thermal annealing significantly reduces the conductivity of the copper-based PLA [37]. The relative difference in resistivity is therefore expected to be greater for copper-based traces compared to carbon-based traces. The resistivity of the 0-degree trace was 0.56 Ω·*mm*. The differences between the highest and the lowest resistivity of the copper-based planar samples and conformal samples was 1831.7 Ω·*mm* and 0.8 Ω·*mm*, respectively.

To investigate the cross-sectional profile of the planarly and conformally printed traces, the 45-degree samples were cast in epoxy resin and saw-cut perpendicularly to the trace's direction. The cross-section was then polished into a smooth surface for imaging. Fig. 10 shows the cross-sectional image of the 45-degree samples: A) Carbon-based PLA printed via planar approach (left) and conformal approach (right); and B) Copper-based PLA printed via planar approach (left) and conformal approach (right). In the figure, the 4 elliptical layers of the extrusion are clearly visible in the conformal deposition, whereas the individual layers appear fused for planar samples. This is due to the geometry of the planarly printed traces in relation to their direction and the cut. The greater the angle of incline, the more individual layers parallel to the cut. Consequently, individual layers appear thicker to the point where fewer than four layers accommodate the cross-sectional area. Interestingly, the sectional profile of the copper-based planar sample shows an even greater interaction between the layers. The cross-section is thinning toward the tip, and the oval shape of individual layers is not obvious. This could be attributed to a dragging effect, also noticed in Fig. 7A, where the retracting nozzle pulls on the deposited material. Due to the short path of the in-layer deposition in planar printing, the effect is much more obvious than in conformal printing. This effect is likely not as noticeable with the carbon-based samples due to the higher print temperature and consequently lower viscosity of the conductive PLA material. Furthermore, this could explain the relatively poorer performance of the copper-based planar sample when compared to the carbon-based planar sample. Additional cross-sectional images for planar samples with 30-degree and 60-degree inclines are shown in Fig. S2 in SM. Using the microscopic image, the cross-sectional area of the conductive traces was measured by counting pixels. Table 2 shows the cross-sectional areas of the traces corresponding to Fig. 10.

4.2. Effect of 5-axis 3D printing on curved surface

Fig. 11 shows the curvature radius samples for carbon-based PLA 3D printed via A) conformal and B) planar approaches. Fig. 12 shows the resistivity of the printed traces. As shown in Table 3, unlike the inclined samples, the layer count does not change as much between each radius, and therefore the measurement shows no obvious relationship between the resistance and the radius. For the conformally printed samples, the resistivity of the traces was consistent throughout all curvature radii, with a much smaller range of values. The most significant difference in resistivity between the planar traces was 42 Ω·mm, and 18.5 Ω·mm for conformal traces.

Fig. 13 shows the curvature radius samples for copper-based PLA 3D printed via A) conformal and B) planar approach. As shown in Fig. 14, the resistivity of the conformal traces is much more consistent in comparison to the planar traces. The difference between the highest and the lowest resistivity for the planar traces was 7.5 Ω·*mm* and 0.8 Ω·*mm* for the conformal traces.

Table 2
Measured cross-sectional area of the 45-degree incline samples.

	Carbon, Planar	Carbon, Conformal	Copper, Planar	Copper, Conformal
Area (mm^2)	0.75	0.79	0.75	0.72
Deviation (mm^2)	0.03	0.07	0.03	0.00
Relative Error (%)	4.8	10	2.1	0.1

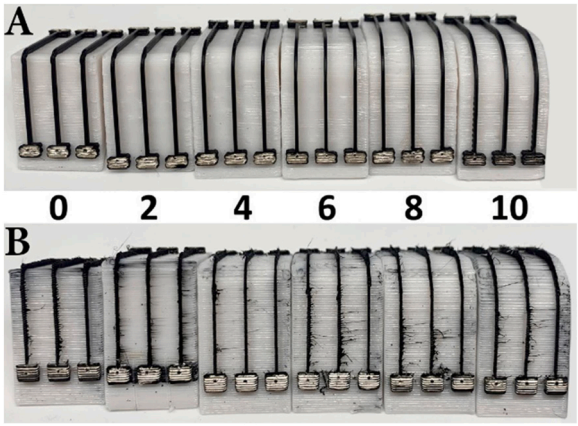

Fig. 11. Carbon-based conductive traces printed onto curved substrate with a curvature radius ranging from 0 to 20 mm. A) samples printed via conformal and B) samples printed via planar approach.

4.3. Effect of substrate surface on conformal trace

Fig. 15 shows the normalised resistivity of the conformal traces in detail for left) the angle of incline, and right) radius of curvature. The normalisation was calculated by dividing the individual data points with the largest data point of each respective data set. In Fig. 15 (left) we can notice that the resistivity of the copper-based traces increases with the angle of incline toward 90 degrees and then drops again at 105 degrees. This change in resistivity resembles the trend shown in the earlier planar

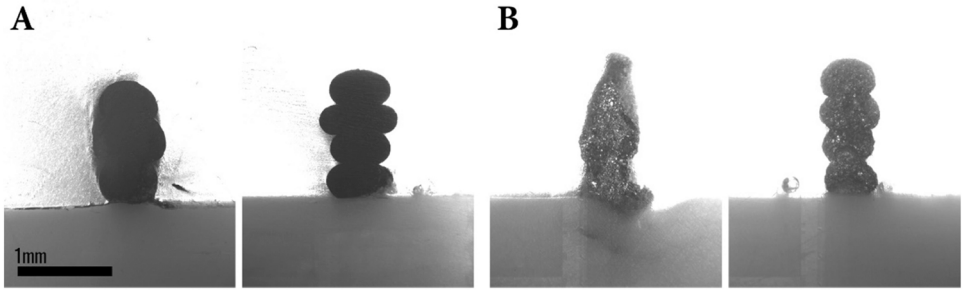

Fig. 10. Cross-sectional images of the 45-degree samples: A) Carbon-based and B) Copper-based. The planar samples are shown on the left, and the conformal samples are on the right. Illustration of the cut-plane is shown in Fig. S3 in SM.

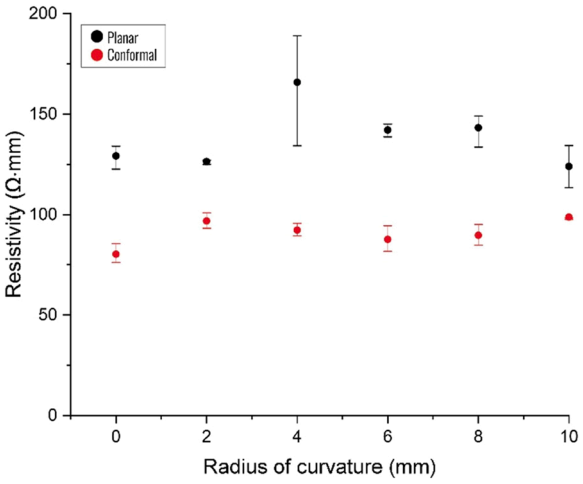

Fig. 12. The average resistivity of the printed carbon-based PLA traces. Planarly printed traces are in black and conformally printed traces are in red. The error bars indicate the range of measured values for the respective radius of curvature.

Table 3
Radius of curvature and number of layers for conductive traces.

Radius (mm)	0	2	4	6	8	10
Number of layers	85	88	86	82	78	74

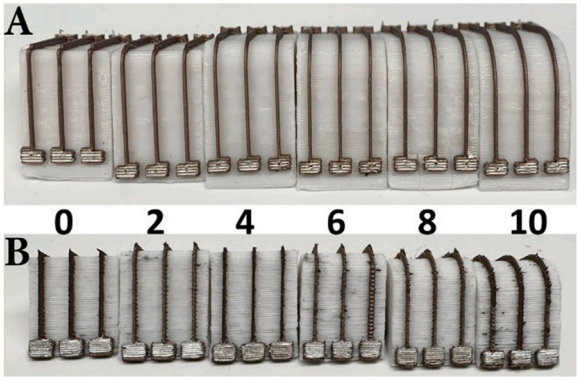

Fig. 13. Copper-based conductive traces printed onto curved substrate with a curvature radius ranging from 0 to 20 mm. A) samples printed via conformal and B) samples printed via planar approach.

sample. However, this trend is likely due to the interaction between the substrate and the conformal trace, in which the substrate's surface geometry influences the conformal trace's resistivity and, as shown in Table 1, the larger the angle of incline, the more layered is the surface that the conformal trace needs to interact with. Unlike the copper-based traces, the carbon-based traces do not appear to be affected by the condition of the substrate's surface. We believe this is due to the material characteristics of the carbon-based PLA being less susceptible to the print settings and print environment. The greatest difference between the highest and the lowest normalised resistivity for copper-based trace was 0.6, whereas, for carbon-based trace, it was 0.2. We also noticed that the normalised resistivity of the curved traces does not show a clear trend for both copper-based and carbon-based traces, as shown in Fig. 15 (right). We believe this is because the curved samples do not have significant change in the number of layers to indicate a clear trend. The greatest differences were 0.35 and 0.2 for copper and carbon-based traces, respectively.

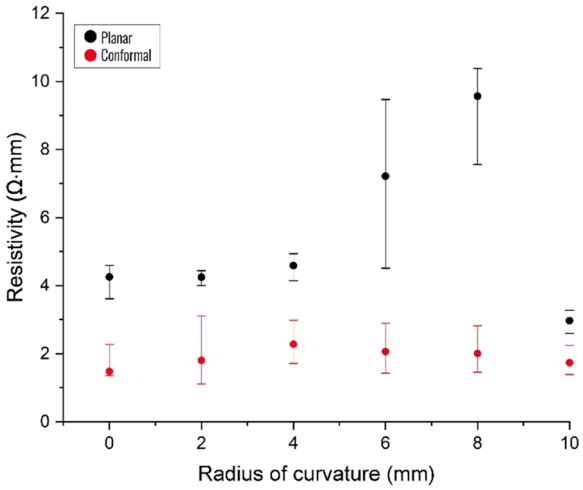

Fig. 14. The average resistivity of the copper-based PLA traces. Planarly printed samples are in black and conformally printed samples are in red. The error bars indicate the range of measured values for the respective radius of curvature.

4.4. Conformal 3D printing onto concave substrate

One of the apparent limitations of conformal 3D printing using 5-axis is that due to the shape of the printing nozzle, it is challenging to deposit material onto a concave surface. As shown in Fig. 16, the 'printability' onto a concave surface is very much dependent on the shape of the elongated nozzle. The smallest curvature radius our machine can print conformally is 6 mm.

Fig. 17 shows carbon-based conductive traces printed onto concave substrates, whose radii ranged from 6 mm to 10 mm. We compared the resistivity of the concave traces to the convex traces. From Fig. 18 we can see that the resistivities of the concave traces are well within the range of convex traces with the corresponding curvature radius. This is expected as the traces are geometrically equivalent.

4.5. Conductive patterns on free-form and doubly curved substrate

In this section, we use the resistivity measured from the inclined samples to estimate the resistance of the more complex conductive pattern on a freeform vase-like substrate. As shown in Fig. 4, the vase-like object has 6 conductive patterns with various shapes and lengths. The actual 3D printed object is shown in the Fig. 19. Using the formula $R = \rho l/A$ we estimated the resistances of each pattern and compared them with the measured resistances. Table 4 shows the values for carbon-based traces and Table 5 shows the values for copper-based traces. The value of resistivity used for estimation was obtained by averaging the resistivity of all conformally printed traces at all angles of incline for the respective material. The error of resistivity was estimated to be half of the average difference between the minimum and maximum for the respective material. As seen in Fig. 15, the relative value range was much higher for copper-based traces than carbon-based ones. Therefore, the error range for the copper-based PLA is more indicative of the dependency of the angle of incline. In contrast, the error range of the carbon-based PLA is more indicative of the variability of the printing process, which can be seen in the variations of the measured cross-sectional area (Table 2 and Table S1). Furthermore, the conformal traces on the vase-like substrate are deposited on the surface that is mostly at a 60–90-degree incline, which can explain why the measured resistance is closer to the upper bound of the estimated resistance for copper-based traces.

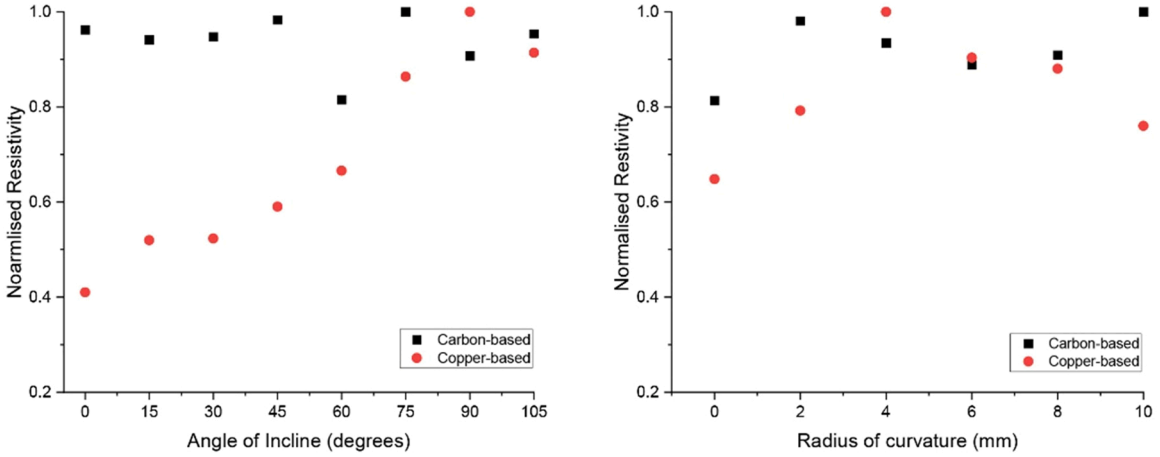

Fig. 15. Normalised resistivity of the conformal traces for angle of incline (left), and Radius of curvature (right).

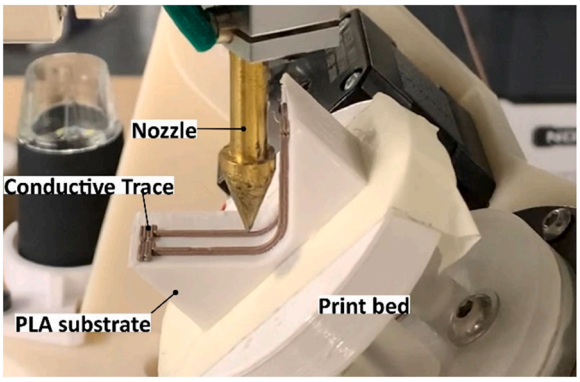

Fig. 16. 5-axis 3D printing on a concave substrate with a 6 mm curvature radius.

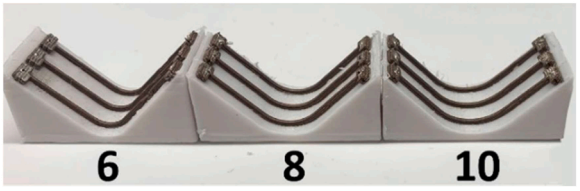

Fig. 17. Conformally 3D printed carbon-based traces for concave curvature radius of 6 mm, 8 mm and 10 mm.

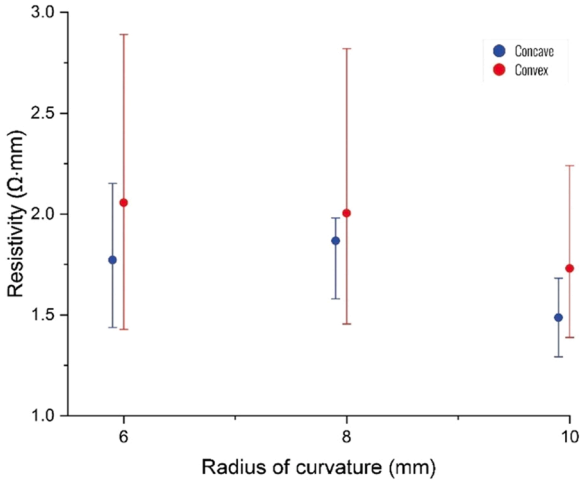

Fig. 18. The average resistivity of the copper-based traces conformally printed onto: Blue) a concave substrate, and Red) a convex surface. Measurements of the concave traces are shifted slightly in x-axis of the graph for improved legibility. The error bars indicate the range of measured values for the respective radius of curvature.

Fig. 19. Conductive traces conformally printed onto vase-like doubly curved substrate. Left) Carbon-based trace; and Right) copper-based trace.

5. Conclusion

This paper demonstrated a method of employing a multi-material 5-axis 3D printer to print conformal electrical traces onto a free-form and arbitrarily curved substrate. The advantages of employing 5-axis 3D printing over the conventional planar process were investigated by comparing the resistivity of the 3D printed traces constructed with conformal and planar approaches. Our study shows that 3D printing conductive traces using a conformal approach significantly stabilises the conductivity of the printed traces for various geometries of the substrate. We found that the most contributing factor to the decreased conductivity of the printed trace is the reliance on inter-layer bonding. This was especially apparent for copper-based PLA. We also noticed that copper-based PLA is indeed more susceptible to the printing environment. This sensitivity has been reported to be a result of redistribution of metallic particles inside the thermoplastic when exposed to different temperature profiles [31]. Furthermore, the rough texture of the substrate surface can also affect the conductivity of the conformal trace. The microscopic image of the printed structure shows clear evidence that the quality of the conformal features can be significantly improved through multi-axis 3D printing, which also eliminates oozing and stringing. We

Table 4
Estimated and measured resistance of the carbon-based conductive pattern on doubly curved vase-like substrate.

Pattern No.	Length (mm)	Estimated Resistance (kΩ)	Measured Resistance (kΩ)
1	116	13.2 ± 1.3	14.0
2	93	10.6 ± 1.0	10.5
3	115	13.1 ± 1.3	12.0
4	131	14.9 ± 1.5	15.3
5	79	9.0 ± 0.9	9.8
6	69	7.9 ± 0.8	8.1

Table 5
Estimated and measured resistances of the copper-based conductive traces on doubly curved vase-like substrate.

Pattern No.	Length (mm)	Estimated Resistance (Ω)	Measured Resistance (Ω)
1	116	152 ± 66	253
2	93	122 ± 53	145
3	115	151 ± 65	178
4	131	172 ± 74	178
5	79	104 ± 45	126
6	69	91 ± 39	112

also showed that we can estimate the resistance of more complex traces on a vase-like substrate based on the resistivity measured from traces printed on various angles of incline. In future work, we will perform mechanical evaluation of 5-axis 3D printed electrical objects against existing standards and proposed techniques specific to additive manufacturing to determine precise adhesion, bending and temperature resistance properties and characteristics.

CRediT authorship contribution statement

Freddie Hong: Writing – original draft, Software, Methodology, Investigation, Formal analysis, Data curation, Conceptualization. **Borut Lampret:** Writing – review & editing, Methodology, Investigation, Formal analysis. **Connor Myant:** Supervision, Resources. **Steve Hodges:** Validation, Supervision. **David Boyle:** Writing – review & editing, Supervision, Resources, Methodology, Formal analysis.

Declaration of Competing Interest

The authors declare that they have no known competing financial interests or personal relationships that could have appeared to influence the work reported in this paper.

Data availability

Data will be made available on request.

Appendix A. Supporting information

Supplementary data associated with this article can be found in the online version at doi:10.1016/j.addma.2023.103546.

References

[1] J.L.C. Jr, K.M. Billah, C.F.A. Carrasco, S.A. Barraza, R.B. Wicker, D. Espalin, "Hybrid manufacturing with FDM technology for enabling power electronics component fabrication,", *Solid Free. Fabr.* (2018) 357–364.

[2] C. Kim, et al., "3D printed electronics with high performance, multi-layered electrical interconnect,", IEEE Access vol. 5 (2017) 25286–25294, https://doi.org/10.1109/ACCESS.2017.2773571.

[3] J.J. Adams, et al., "Conformal printing of electrically small antennas on three-dimensional surfaces,", issn: 09359648, Adv. Mater. vol. 23 (11) (2011) 1335–1340, https://doi.org/10.1002/adma. 201003734.

[4] F. Wasserfall, "Embedding of SMD populated circuits into FDM printed objects,", SFF Symp. Proc. (2015) 180–189.

[5] A.J. Lopes, E. MacDonald, R.B. Wicker, "Integrating stereolithography and direct print technologies for 3D structural electronics fabrication,", issn: 13552546, Rapid Prototyp. J. vol. 18 (2) (2012) 129–143, https://doi.org/10.1108/13552541211212113.

[6] F. Wasserfall, N. Hendrich, D. Ahlers, J. Zhang, "Topology-aware routing of 3D-printed circuits,", issn: 22148604, Addit. Manuf. vol. 36 (April) (2020), 101523, https://doi.org/10.1016/j.addma.2020.101523.

[7] P.F. Flowers, C. Reyes, S. Ye, M.J. Kim, B.J. Wiley, "3D printing electronic components and circuits with conductive thermoplastic filament,", issn: 22148604, Addit. Manuf. vol. 18 (2017) (2017) 156–163, https://doi.org/10.1016/j.addma.2017.10.002.

[8] Y. Song, R.A. Boekraad, L. Roussos, A. Kooijman, C.C.L. Wang, and J.M.P. Geraedts, "3D Printed Electronics: Opportunities and Challenges From Case Studies," in *"3D Printed Electronics: Opportunities and Challenges From Case Studies." Proceedings of the ASME 2017 International Design Engineering Technical Conferences and Computers and Information in Engineering Conference. Volume 1: 37th Computers and Information*, Cleveland, Ohio, USA, 2017. [Online]. Available: https://doi.org/10.1115/DETC2017–67503.

[9] K. Sim, et al., "Three-dimensional curvy electronics created using conformal additive stamp printing,", issn: 25201131, Nat. Electron. vol. 2 (10) (2019) 471–479, https://doi.org/10.1038/s41928019-0304-4. issn: 25201131. doi: ⟨https://doi.org/10.1038/s41928-019-0304-4⟩.

[10] G. Saada, M. Layani, A. Chernevousky, S. Magdassi, "Hydroprinting Conductive Patterns onto 3D Structures,", issn: 2365709X. doi: Adv. Mater. Technol. vol. 2 (5) (2017) 1–6, https://doi.org/10.1002/admt.201600289.

[11] D. Groeger, J. Steimle, "ObjectSkin: augmenting everyday objects with hydroprinted touch,", Proc. ACM Interact., Mob., Wearable Ubiquitous Technol. vol. 1 (4) (2018) 1–23, issn: 24749567. doi: 10.1145/3161165. [Online]. Available: ⟨http://dl.acm.org/citation.cfm?doid=3178157.3161165⟩.

[12] L.W.T. Ng, et al., "Conformal printing of graphene for single- and multilayered devices onto arbitrarily shaped 3D surfaces,", issn: 16163028, Adv. Funct. Mater. vol. 29 (36) (2019), https://doi.org/10.1002/adfm.201807933.

[13] F. Hong, C. Myant, and D.E. Boyle, "Thermoformed Circuit Boards: Fabrication of Highly Conductive Freeform 3D Printed Circuit Boards with Heat Bending," in *Proceedings of the 2021 CHI Conference on Human Factors in Computing Systems*, New York, NY, USA: Association for Computing Machinery, 2021, isbn: 9781450380966. [Online]. Available: https://doi.org/10.1145/3411764.3445469.

[14] F. Hong, L. Tendera, C. Myant, D. Boyle, "Vacuum-formed 3D printed electronics: fabrication of thin, rigid and free-form interactive surfaces,", issn: 26618907, SN Comput. Sci. vol. 3 (4) (2022) 1–12, https://doi.org/10.1007/s42979-022-01174-1.

[15] Optomec Aerosol Jet printing technology effectively produces 3D printed electronics. [Online]. Available: ⟨https://optomec.com/printed-electronics/aerosol-jet-%20technology/⟩.

[16] B. Urasinska-Wojcik, et al., "Integrated manufacture of polymer and conductive tracks for realworld applications,", issn: 22148604, Addit. Manuf. vol. 29 (July) (2019), 100777, https://doi.org/10.1016/j.addma.2019.06.028.

[17] P.M. Bhatt, R.K. Malhan, P. Rajendran, S.K. Gupta, "Building free-form thin shell parts using supportless extrusion-based additive manufacturing,", issn: 22148604, Addit. Manuf. vol. 32 (October 2019) (2020), 101003, https://doi.org/10.1016/j.addma.2019.101003.

[18] P.M. Bhatt, R.K. Malhan, A.V. Shembekar, Y.J. Yoon, S.K. Gupta, "Expanding capabilities of additive manufacturing through use of robotics technologies: A survey,", issn: 22148604, Addit. Manuf. vol. 31 (November 2019) (2020), 100933, https://doi.org/10.1016/j.addma.2019.100933.

[19] J.A. Gardner, N. Kaill, R.I. Campbell, G.A. Bingham, D.S. Engstrøm, and N.O. Balc, "Aligning Material Extrusion Direction with Mechanical Stress via 5-Axis Tool Paths," in *29th Annual International Solid Freeform Fabrication Symposium - An Additive Manufacturing Conference, SFF 2018* , 2018, pp. 2005–2019.

[20] F. Hong, S. Hodges, C. Myant, and D.E. Boyle, "Open5x: Accessible 5-axis 3D printing and conformal slicing," *Conference on Human Factors in Computing Systems - Extended Abstract*, 2022. doi: 10.1145/3491101.3519782.

[21] M.A. Isa, I. Lazoglu, "Five-axis additive manufacturing of freeform models through buildup of transition layers,", issn: 02786125, J. Manuf. Syst. vol. 50 (December 2018) (2019) 69–80, https://doi.org/10.1016/j.jmsy.2018.12.002.

[22] R.K. Muller, https://xyzdims.com, 2022–3-16. [Online]. Available: ⟨https://xyzdims.com/2021/02/08/3d-printing-penta-axis-pax-5-axis-printing-option/⟩.

[23] Ø.K. Grutle, "5-axis 3D Printer," Ph.D. dissertation, University of Oslo, 2015, p. 96. [Online]. Available: ⟨https://www.duo.uio.no/handle/10852/47652⟩.

[24] F. Alkadi, K.C. Lee, A.H. Bashiri, J.W. Choi, "Conformal additive manufacturing using a direct-print process,", issn: 22148604, Addit. Manuf. vol. 32 (November 2019) (2020), 100975, https://doi.org/10.1016/j.addma.2019.100975.

[25] S. Singamneni, A. Roychoudhury, O. Diegel, B. Huang, "Modeling and evaluation of curved layer fused deposition,", issn: 09240136, J. Mater. Process. Technol. vol. 212 (1) (2012) 27–35, https://doi.org/10.1016/j.jmatprotec.2011.08.001.

[26] Rhino, 5xMonkey 5-axis CAM for RhinoGrasshopper. [Online]. Available: http://www.5axismaker. com/software/.

[27] S. Lim, R.A. Buswell, P.J. Valentine, D. Piker, S.A. Austin, X. De Kestelier, "Modelling curved-layered printing paths for fabricating large-scale construction components,", issn: 22148604, Addit. Manuf. vol. 12 (2016) 216–230, https://doi.org/10.1016/j.addma.2016.06.004.

[28] G. Venturini, F. Montevecchi, F. Bandini, A. Scippa, G. Campatelli, "Feature based three axes computer aided manufacturing software for wire arc additive

manufacturing dedicated to thin walled components,", issn: 22148604, Addit. Manuf. vol. 22 (March) (2018) 643–657, https://doi.org/10.1016/j.addma.2018.06.013.
[29] ProtoPasta, 2022–03-31. [Online]. Available: ⟨https://www.proto-pasta.com/pages/conductivepla⟩.
[30] Multi3D, 2022–03-31. [Online]. Available: ⟨https://www.multi3dllc.com/faqs/⟩.
[31] J.A. Cardenas, et al., "Flash ablation metallization of conductive thermoplastics,", issn: 2214-8604, Addit. Manuf. vol. 36 (June) (2020), 101409, https://doi.org/10.1016/j.addma.2020.101409.
[32] E3D, *E3D ToolChanger, 2022–03-31*. [Online]. Available: https://e3d-online.com/pages/ toolchanger.
[33] Duet3D, Duet 2 WiFi and Ethernet Hardware Overview, 2022–01-12. [Online]. Available: ⟨https://docs.duet3d.com/Duet3D_hardware/Duet_2_family/Duet_2_WiFi_Ethernet_Hardware_Overview⟩.
[34] RepRapFirmware. [Online]. Available: ⟨https://www.reprapfirmware.org/⟩.
[35] A. Gleadall, "FullControl GCode Designer: Open-source software for unconstrained design in additive manufacturing,", issn: 22148604, Addit. Manuf. vol. 46 (June) (2021), 102109, https://doi.org/10.1016/j.addma.2021.102109.
[36] D.B. Perez, E. Celik, R.L. Karkkainen, "Investigation of interlayer interface strength and print morphology effects in fused deposition modeling 3D-printed PLA,", 3D Print. Addit. Manuf. vol. 8 (1) (2021) 23–32, https://doi.org/10.1089/3dp.2020.0109 ([Online]. Available), ⟨https://doi.org/10.1089/3dp.2020.0109⟩.
[37] J.A. Cardenas, et al., "Flash ablation metallization of conductive thermoplastics,", issn: 22148604, Addit. Manuf. vol. 36 (March) (2020), 101409, https://doi.org/10.1016/j.addma.2020.
[38] Nathan Lazarus and Sarah S. Bedair, "Creating 3D printed sensor system with conductive composite," *2021 Smart Mater. Struct.* 30 015020. doi: 10.1088/1361–665X/abcbe2.
[39] H. Gao, N.A. Meisel, Exploring the manufacturability and resistivity of conductive filament used in material extrusion additive manufacturing, Solid Free. Fabr. 2017 Proc. 28th Annu. Int. Solid Free. Fabr. Symp. - An Addit. Manuf. Conf. SFF 2017, 2020: 1612–1626.
[40] M.O.F. Emon, et al., 'Multi-material 3D printing of a soft pressure sensor', Addit. Manuf. 28 (May) (2019) 629–638, https://doi.org/10.1016/j.addma.2019.06.001.
[41] M. Vatani, E.D. Engeberg, J.W. Choi, 'Conformal direct-print of piezoresistive polymer/nanocomposites for compliant multi-layer tactile sensors', Addit. Manuf. 7 (2015) 73–82, https://doi.org/10.1016/j.addma.2014.12.009.
[42] G. Fang, T. Zhang, S. Zhong, X. Chen, Z. Zhong, C.C.L. Wang, Reinforced FDM: Multi-axis filament alignment with controlled anisotropic strength, ACM Trans. Graph. 39 (2020), https://doi.org/10.1145/3414685.3417834.
[43] T. Zhang, G. Fang, Y. Huang, N. Dutta, S. Lefebvre, Z.M. Kilic, C.C.L. Wang, S3-Slicer: A General Slicing Framework for Multi-Axis 3D Printing, ACM Trans. Graph. 41 (2022), https://doi.org/10.1145/3550454.3555516.